Thermodynamic Control of Activity Patterns in Cytoskeletal Networks

Alexandra Lamtyugina,[1] Yuqing Qiu,[1,2] Étienne Fodor,[3]
Aaron R. Dinner,[1,2] and Suriyanarayanan Vaikuntanathan[1,2,*]
[1]Department of Chemistry, University of Chicago, Chicago, Illinois 60637, USA
[2]James Franck Institute, University of Chicago, Chicago, Illinois 60637, USA
[3]Department of Physics and Materials Science, University of Luxembourg, L-1511 Luxembourg, Luxembourg

(Received 31 January 2022; accepted 26 July 2022; published 16 September 2022)

Biological materials, such as the actin cytoskeleton, exhibit remarkable structural adaptability to various external stimuli by consuming different amounts of energy. In this Letter, we use methods from large deviation theory to identify a thermodynamic control principle for structural transitions in a model cytoskeletal network. Specifically, we demonstrate that biasing the dynamics with respect to the work done by nonequilibrium components effectively renormalizes the interaction strength between such components, which can eventually result in a morphological transition. Our work demonstrates how a thermodynamic quantity can be used to renormalize effective interactions, which in turn can tune structure in a predictable manner, suggesting a thermodynamic principle for the control of cytoskeletal structure and dynamics.

DOI: 10.1103/PhysRevLett.129.128002

The actin cytoskeleton is a paradigmatic example of an adaptive biomaterial that regulates important biophysical properties of the cell, such as its structural integrity, motility, and signaling, by adopting various nonequilibrium morphologies [1–3]. While there have been many efforts to unravel the driving forces responsible for sustaining many of these structures [1,4–9], a clear thermodynamic understanding of the underlying principles governing their adaptive properties has remained elusive [10]. Here, using tools from large deviation theory [11], we provide evidence that a nonequilibrium thermodynamic control framework can indeed predict and rationalize adaptive structural transitions in cytoskeletal networks. Specifically, the central question motivating our work is this: Can we predict how a cytoskeletal network adapts its structure to external conditions (e.g., conditions requiring the formation of a contractile bundle) by controlling its energy budget?

To answer this question, we introduce a model that resembles *in vitro* biomaterials consisting of actin filaments and molecular motors [Fig. 1(a)], and exhibits two well-known phases of such assemblies: asters and bundles [Fig. 1(b)] [2,4]. The core of the bundles is composed of antiparallel actin strands resembling morphologies found in stress fibers and cytokinetic rings [12,13]. The transition between these two states can be achieved in our model by modulating a material parameter related to the motor stiffness. Our main result shows how, by controlling the statistics of the rate of work done by the motors, the cytoskeletal network can transition between asters and bundles, thus generating configurations characteristic of different microscopic material properties. Importantly, this transition is achieved even when the microscopic makeup of the cytoskeletal material (i.e., motor stiffness, motor speed, filament concentrations) are all held fixed.

We obtain our results by building on recent theoretical studies [11,14–17] based on large deviation theory [18,19] and stochastic thermodynamics [17,20,21] and applying them to our model actomyosin system. The framework of large deviation theory provides a convenient way to control the rate of work by applying a dynamical bias to an ensemble of trajectories, namely a series of time realizations for the coordinates of motors and filaments. Combining simulations with phenomenological theory, we reveal that the configurations generated with such a dynamical bias resemble those that would have been generated with a specific renormalization of the microscopic material properties. Specifically, for the regimes investigated here, given a cytoskeletal biomaterial composed of filaments and motors with a set stiffness and biochemical makeup, we show how configurations characteristic of different values of motor stiffness can be accessed by simply modulating the statistics of the work done by the motors.

Our results suggest that controlling the rate of work, which could be achieved in practice by changing the consumption of chemical fuel [22,23], can be regarded as a basic design principle for the development of an adaptive biomaterial. Below, we first introduce the microscopic coarse-grained description of actomyosin networks that we use in this Letter. Next, we introduce tools of large deviation theory, such as trajectory biasing, that allow us to probe the response of the system as the statistics of the work done by the motor are tuned. Finally, our main results in Fig. 2 demonstrate how a biomaterial can access different classes of configurations, even though its microscopic

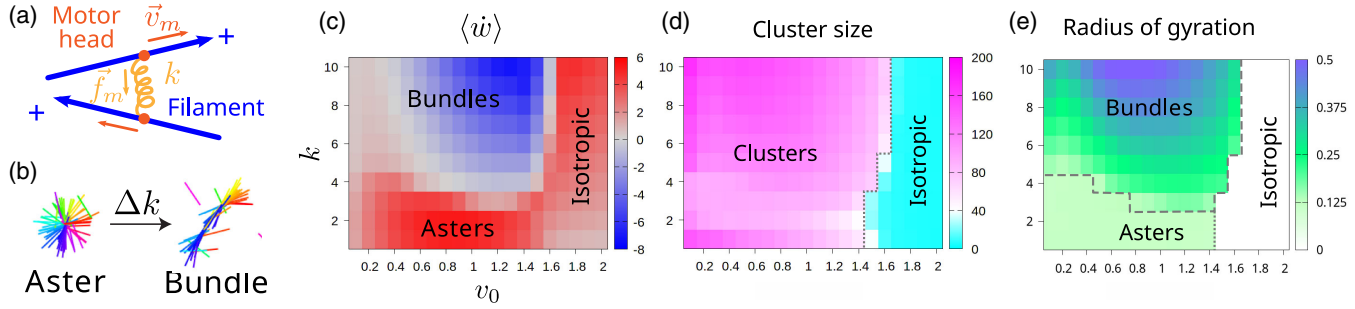

FIG. 1. Structural transition between asters and bundles. (a) Schematic of two filaments (blue) connected by a motor (orange). The motor is modeled as a Hookean spring with rigidity k. The motor force $|\vec{f}_m|$ is proportional to motor rigidity k. Each motor head (dark orange) binds to one filament and moves toward the barbed (+) end with velocity $\vec{v}_m$ [Eq. (1)]. When the motor is bound to two filaments, the rate of work done by the motor spring ($\dot{w}$) is computed as the sum of $\vec{f}_m \cdot \vec{v}_m$ over the two motor heads. (b) Tuning k induces the structural transition between asters and bundles. (c) Color map of $\langle \dot{w} \rangle$. Asters and bundles are respectively associated with positive and negative values of $\langle \dot{w} \rangle$. (d) Color map of the largest cluster size. A system with no cluster larger than 40 is considered to be isotropic. (e) Color map of radius of gyration R_g, of the largest cluster. The boundary between the bundle and aster regions $R_g = 0.125$. The boundary of the isotropic region is the same as in (d).

makeup remains the same, when tuning the statistics of the work done by molecular motors.

Inspired by the rich phase diagram exhibited by actomyosin systems both *in vivo* [24] and *in vitro* [2,4,25], we study the organization of short polar filaments connected by molecular motors using a coarse-grained platform, CYTOSIM [26]. Actin filaments and motors are, respectively, modeled as semiflexible polymers and Hookean springs with filament binding sites at the two ends [Fig. 1(a)]. Each motor head can bind to a filament and walk along its length toward the barbed end. When both motor heads are bound, the spring exerts a force $\vec{f}_m$ on the motor head in the direction pointing from the motor head to the center of the motor. The magnitude of $\vec{f}_m$ is determined by the motor rigidity, k, and the length of the spring, l: $|\vec{f}_m| = kl$. This force then modulates the loaded speed of each motor head v_m as [26]

$$v_m = v_0(1 + \vec{f}_m \cdot \hat{d}/f_0), \tag{1}$$

where $\hat{d}$ is the unit vector pointing from the motor head to the barbed end of the filament, f_0 and v_0 are the friction force and velocity constants, respectively. As the motor heads walk along the filaments, they transmit the forces originating from the motor springs, and in response, the actin filaments can assemble into specific structures.

The phase diagram obtained by tuning the motor rigidity k and the motor unloaded velocity v_0 is described in Figs. 1(c)–1(e). We characterize various regimes by calculating the size of the largest cluster of the filament-motor cluster [Fig. 1(d)], and its radius of gyration R_g [Fig. 1(e), Sec. S1C of Supplemental Material [27]]. Values of R_g larger than half the length of a single filament indicate elongated bundlelike structures. Long bundles form at large k, and decreasing k reduces R_g until it reaches a plateau value corresponding to a radial arrangement of filaments, namely asters (Figs. S1 and S2). This trend is consistent across different values of v_0 (Fig. S2). Neither bundles nor asters form when the unloaded motor velocity v_0 exceeds a critical value, in which case a diffuse isotropic phase is observed. Our asters and bundles share core characteristics with those observed in experiments, such as the antiparallel alignment of filaments in sarcomeric bundles and stress fibers [31] and clusters of radial filaments *in vitro* [1,32] (Fig. S1).

The rate of work due to the relative motion of the motor on the actin filament is defined as

$$\dot{w} = \sum_m \vec{f}_m \cdot \vec{v}_m, \tag{2}$$

where m runs over the number of motor heads [Fig. 1(a)]. In what follows, we focus on the range of v_0 where the bundle-aster transition occurs, which is associated with a change of sign of the average rate of work $\langle \dot{w} \rangle$ [Fig. 1(c)]. In this regime, we aim to demonstrate that the transitions and structural changes that can be achieved by modulating the motor stiffness can equivalently be achieved, even when the motor stiffness and other material properties are held fixed, by modulating the statistics of $\dot{w}$ using tools from large deviation theory.

Specifically, we bias the trajectories generated in our simulations according to the rate of work (using the cloning algorithm [33,34]; see Sec. S1E) such that the probability of biased trajectories reads

$$\mathcal{P}_\alpha \propto \mathcal{P}_0 e^{\alpha \int_0^\tau \dot{w} dt}, \tag{3}$$

where $\mathcal{P}_0$ is the probability of the trajectory in the absence of biasing, and τ is the duration of the trajectories. The parameter α tunes the strength and direction of the bias.

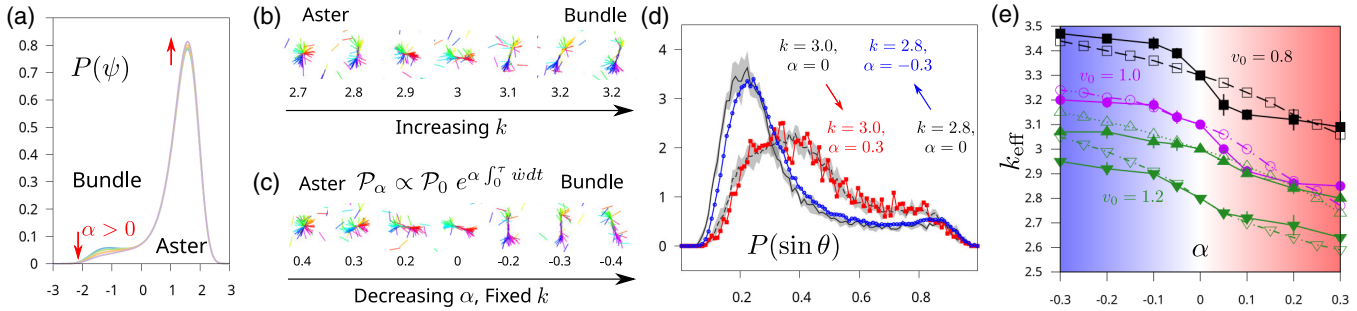

FIG. 2. Dynamical bias effectively renormalizes the motor rigidity k. (a) Probability distribution obtained by biasing the dynamics of a given order parameter ψ (with free energy $\mathcal{F}(\psi) = -a\psi + b\psi^2 - c\psi^3 + d\psi^4$) with respect to ψ. Parameters: $a = 4d = -b = -30c = 1$. Biasing parameter: $\alpha = 0$ (unbiased dynamics, blue), 0.005 (green), 0.1 (orange), and 0.3 (purple). (b) Snapshots of unbiased simulations with changing motor rigidity k. (c) Snapshots of biased simulations with fixed motor rigidity $k = 3$. (d) The statistics of structures from biased dynamics match that from an unbiased simulation at a different k. The order parameter $\sin\theta$ is calculated from angles between neighboring filaments and averaged across nearest neighbors. Matching the distribution of $\sin\theta$ from biased (black lines with the error bar shown with gray area) and unbiased simulations (red and blue) results in defining an effective rigidity k_{eff}. (e) Effective rigidity k_{eff} as a function of bias parameter α at $v_0 = 0.8$ (black), 1.0 (magenta), and 1.2 (green). The two green curves correspond to $k = 3$ and 2.8 analyzed for $v_0 = 1.2$. Filled points are obtained by matching structures from biased and unbiased simulations. Hollow points are analytical predictions derived from the two-state model [Eq. (7)].

In practice, trajectory biasing against the rate of work $\dot{w}$ can be considered as a way to probe the response of the system as the statistics of $\dot{w}$ are tuned [19]. Besides, the specific choice of exponential reweighting in Eq. (3) ensures that the distance between original and biased dynamics, as measured by the Kullback-Leibler divergence of their respective trajectory probabilities, is minimal [19]. Below, we show that the configurations accessed when tuning the statistics of $\dot{w}$ resemble those that would have naturally emerged in a material with a renormalized motor rigidity k.

Before proceeding to our numerical results, we first motivate how applying dynamical bias might impact system properties by considering a minimal phenomenological model of an actomyosin network [35]. Focusing on a simpler transition between an isotropic state and a state with asters, we show in Sec. S2 that the dynamics of a relevant order parameter, ψ, may be described in terms of an effective free energy landscape $\mathcal{F}(\psi) = -a\psi + b\psi^2 - c\psi^3 + d\psi^4$, with $\{a, b, c, d\}$ as phenomenological parameters. Importantly, the phenomenological terms b and c are modulated by microscopic material constants such as k and v_0, which can explain how the transition from the isotropic state to aster can be achieved by tuning the analogue of the motor rigidity in the phenomenological model (Sec. S2). Furthermore, we show how the application of a trajectory bias $e^{\alpha \int_0^\tau g(\psi) dt}$ results in dynamics that, at small noise, are equivalent to those generated by an effective free energy landscape [34,36] but with renormalized phenomenological constants (Sec. S2B). The probability distributions generated by biasing with various values of α are shown in Fig. 2(a).

This simple perturbative analysis reveals how an application of the bias can renormalize the phenomenological constants b and c, effectively altering the motor rigidity. It also reveals how structural transitions obtained by tuning k might also be achieved by tuning α. This phenomenological model makes it reasonable to speculate that biasing the statistics of $\dot{w}$ in our coarse-grained simulations might effectively change the motor spring stiffness, opening up a different route to a structural transition. To confirm this intuition, we report in Figs. 2(b) and 2(c) snapshots of the structure obtained in the biased dynamics without changing motor rigidity k (Sec. S1E), along with those of unbiased simulations with varying k. The similarity between these structural changes shows that biasing against $\dot{w}$ alone is indeed sufficient to induce the filament-motor system to move across the bundle-aster phase boundary. It also suggests that biasing as in Eq. (3) might be effectively equivalent to modulating motor rigidity.

To quantify the effect of biasing on structure, we measure the relative alignment of filaments through the order parameter $\sin\theta$, where θ is the angle between neighboring filaments. We evaluate the order parameter by averaging $\sin\theta$ over the nearest neighbors for each filament (Sec. S1F). The distribution, $P(\sin\theta)$, is shown for all filaments in the largest filament-motor cluster [Fig. 2(d)]. For bundles at large k, the peak at $\sin\theta \approx 0.25$ reflects parallel orientation of filaments. The distribution shifts toward larger values of $\sin\theta$ as k decreases and the filaments rearrange into an aster. This order parameter $\sin\theta$ is related to the radius of gyration R_g used to illustrate structural changes in Fig. 1(e), but they are not equivalent. $\sin\theta$ is more sensitive to the aster-bundle transition (Sec. S1F). Therefore, we use $\sin\theta$ to quantify the effect of biasing. For each biasing parameter α, we define the effective motor rigidity k_{eff} by matching the distribution $P(\sin\theta)$ measured in the biased dynamics with the distributions obtained in the unbiased dynamics at $k = k_{\text{eff}}$.

In practice, this matching is done by minimizing the divergence between these two distributions (Sec. S1G), leading to a very good agreement between them [Fig. 2(d)]. Repeating this operation for different values of bias parameter α and unloaded motor velocity v_0, we obtain Fig. 2(e), which recapitulates the effect on the system structure of biasing the dynamics. This correspondence confirms that the effect of biasing against the rate of work is indeed fully accounted for as an effective change of motor rigidity, all other parameters being equal.

Finally, since varying motor rigidity k at fixed velocity v_0 leads to a transition between two distinct morphological states, asters and bundles, we aim at constructing a two-state model that, although minimal, is sufficient to rationalize quantitatively the effect of dynamical bias. We begin by assuming that the dynamics associated with the transition can be described by a master equation $\dot{P} = \boldsymbol{W}P$, where P is the column vector with elements $\{P_{\text{aster}}, P_{\text{bundle}}\}$, and $\boldsymbol{W}$ is the transition rate matrix:

$$\boldsymbol{W} = \begin{bmatrix} -R_{ab} & R_{ba} \\ R_{ab} & -R_{ba} \end{bmatrix}. \tag{4}$$

The entries R_{ab} and R_{ba} are meant to model the transition rates from aster to bundle and from bundle to aster, respectively. We express these rates using the Arrhenius law, $R_{ab} = A\exp[-\beta\varepsilon_{\text{bundle}}]$ and $R_{ba} = A\exp[-\beta\varepsilon_{\text{aster}}]$, where the energies of aster and bundle states are given by $\varepsilon_{\text{aster}}$ and $\varepsilon_{\text{bundle}}$, respectively, and A is an Arrhenius prefactor. For convenience, we work in units such that $A = 1$ and $\beta = 1/(k_B T) = 1$, and we set $\varepsilon_{\text{bundle}} = 0$. To quantitatively connect this two-level picture with the simulation results of CYTOSIM, we relate energy levels to distributions by

$$\varepsilon_{\text{aster}} = -\ln\frac{P_{\text{aster}}}{1 - P_{\text{aster}}}, \tag{5}$$

where P_{aster} is extracted from numerical data as $\int_{\sin\theta_c}^{1} P(\sin\theta)d\sin\theta$ with the choice $\sin\theta_c = 0.6$; see Fig. 2(d).

The effect of applying a dynamical bias with respect to $\dot{w}$ is then recapitulated in terms of the master equation $\dot{P}^{(\alpha)} = \boldsymbol{W}^{(\alpha)}P^{(\alpha)}$. The transition matrix $\boldsymbol{W}^{(\alpha)}$ reads

$$\boldsymbol{W}^{(\alpha)} = \begin{bmatrix} -R_{ab} + \alpha\dot{w}_{\text{aster}} & R_{ba} \\ R_{ab} & -R_{ba} + \alpha\dot{w}_{\text{bundle}} \end{bmatrix}, \tag{6}$$

where $\dot{w}_{\text{aster}}$ and $\dot{w}_{\text{bundle}}$ are the rate of work for the aster and bundle states, respectively. The biased transition matrix is known as a "tilted" matrix, and is constructed based on the principles of large deviation theory [18,37] (Sec. S3A). We show that, to leading order in the bias α (Sec. S3B), the effective energy level in biased dynamics $\varepsilon^{(\alpha)}_{\text{aster}}$ can be expressed as [17]

$$\varepsilon^{(\alpha)}_{\text{aster}} \approx \varepsilon_{\text{aster}} - \alpha\frac{(\dot{w}_{\text{aster}} - \dot{w}_{\text{bundle}})}{1 + R_{ba}}. \tag{7}$$

Equation (7) hence predicts how the energy barriers may be modified due to biasing α. This equation can be used to obtain a prediction for k_{eff} as a function of α by substituting the estimate of the modified barrier into Eq. (5) and looking up the value of k at which the estimate of P_{aster} best matches the modified barrier height. The quantity $\dot{w}_{\text{aster}} - \dot{w}_{\text{bundle}}$ in Eq. (7) is best estimated from numerical values of $\langle\dot{w}\rangle$ close to the aster-bundle transition. To generalize this relation to regions away from the transition, we look to the meaning of $\dot{w}_{\text{aster}}$ and $\dot{w}_{\text{bundle}}$ in our two-state model. Specifically, these quantities are meant to denote the typical values of $\dot{w}$ in the regimes of high and low $\sin\theta$, respectively. Since away from this transition, the distribution $P(\sin\theta)$ is dominated by either the bundle or the aster phase, the difference in the typical values of $\dot{w}$ at high and low $\sin\theta$ is reduced. To effectively capture this reduction, we assume that, to leading order, $\dot{w}_{\text{aster}} - \dot{w}_{\text{bundle}}$ is proportional to the slope of the $\dot{w}$ versus k curve, with the proportionality constant as a fitting parameter. This assumption, along with numerical estimates of $\varepsilon_{\text{aster}}$ for a range of k values, enable us to predict how k_{eff} changes with the biasing parameter α (Sec. S3). Our prediction is in good agreement with k_{eff} obtained numerically by directly matching the structure distributions taken from the biased and unbiased dynamics [Fig. 2(e)]. This agreement shows that our two-state model, although providing an oversimplified picture of the underlying dynamics, indeed captures the effective modulation of motor rigidity due to biasing the dynamics with respect to the rate of work.

A feature of probing the response of the system to $\dot{w}$ modulation in this manner (using the tools of large deviation theory) is that we do not provide any explicit protocol for how to perturb the energy consumption. We envision that experiments can be done by deploying active components such as light-sensitive motors [6,8], or by fueling the system with different adenosine triphosphate supplies [22,23], which might provide a physical route for achieving such a perturbation. Our central results hence suggest a new route for the modulation of cytoskeletal material properties through the regulation of underlying energy consumption.

The ideas presented here are complementary to existing hydrodynamic treatments of actomyosin networks [38,39]. These seminal works have shown how various actomyosin phases may be accessed by tuning phenomenological parameters, which in turn affects energy consumption (although in a way that can prove difficult to predict). Instead, our results reveal that *directly* tuning energy consumption, now in a much more predictable manner, is also a route to inducing structural transitions. While we focus here on the connection between $\dot{w}$ and network structure, our work may also provide a road map for

understanding how cytoskeletal networks adapt to changing external stress conditions. Indeed, when the motor head velocity is a constant, $\dot{w}$ is simply proportional to the force exerted by motors along the axis of the actin filament [Eq. (2)]. In these regimes, tuning the statistics of $\dot{w}$ is equivalent to tuning the axial forces exerted on the filaments. From a biological perspective, our work paves the way toward a thermodynamic understanding of the control principles regulating the cytoskeleton, to rationalize both how it adapts its structure to external cues [6,8] and how spontaneous flows can form as a result of internal activity [40].

This work was mainly supported by a DOE BES Grant No. DE-SC0019765 through funding to S. V. and Y. Q. Y. Q. was also supported by a Yen Fellowship. A. L. is supported by a NSF Graduate Research Fellowship No. DGE-1746045. E. F. was funded by the Luxembourg National Research Fund (FNR), Grant Reference No. 14389168. A. R. D. acknowledges support from National Institutes of Health Grant No. R35 GM136381 and National Science Foundation Grant No. MCB 2201235.

A. L. and Y. Q. contributed equally to this work.

*Corresponding author.
svaikunt@uchicago.edu

[1] Samantha Stam, Simon L. Freedman, Shiladitya Banerjee, Kimberly L. Weirich, Aaron R. Dinner, and Margaret L. Gardel, Filament rigidity and connectivity tune the deformation modes of active biopolymer networks, Proc. Natl. Acad. Sci. U.S.A. **114**, E10037 (2017).

[2] Simon L. Freedman, Glen M. Hocky, Shiladitya Banerjee, and Aaron R. Dinner, Nonequilibrium phase diagrams for actomyosin networks, Soft Matter **14**, 7740 (2018).

[3] Ulrich S. Schwarz and Margaret L. Gardel, United we stand–integrating the actin cytoskeleton and cell–matrix adhesions in cellular mechanotransduction, J. Cell Sci. **125**, 3051 (2012).

[4] Darius Vasco Köster, Kabir Husain, Elda Iljazi, Abrar Bhat, Peter Bieling, R. Dyche Mullins, Madan Rao, and Satyajit Mayor, Actomyosin dynamics drive local membrane component organization in an in vitro active composite layer, Proc. Natl. Acad. Sci. U.S.A. **113**, E1645 (2016).

[5] Kimberly L. Weirich, Kinjal Dasbiswas, Thomas A. Witten, Suriyanarayanan Vaikuntanathan, and Margaret L. Gardel, Self-organizing motors divide active liquid droplets, Proc. Natl. Acad. Sci. U.S.A. **116**, 11125 (2019).

[6] Rui Zhang, Steven A. Redford, Paul V. Ruijgrok, Nitin Kumar, Ali Mozaffari, Sasha Zemsky, Aaron R. Dinner, Vincenzo Vitelli, Zev Bryant, Margaret L. Gardel *et al.*, Spatiotemporal control of liquid crystal structure and dynamics through activity patterning, Nat. Mater. **20**, 875 (2021).

[7] Yuqing Qiu, Michael Nguyen, Glen M. Hocky, Aaron R. Dinner, and Suriyanarayanan Vaikuntanathan, A strong nonequilibrium bound for sorting of cross-linkers on growing biopolymers, Proc. Natl. Acad. Sci. U.S.A. **118**, e2102881118 (2021).

[8] Tyler D. Ross, Heun Jin Lee, Zijie Qu, Rachel A. Banks, Rob Phillips, and Matt Thomson, Controlling organization and forces in active matter through optically defined boundaries, Nature **572**, 224 (2019).

[9] Bezia Lemma, Noah P. Mitchell, Radhika Subramanian, Daniel J. Needleman, and Zvonimir Dogic, Active microphase separation in mixtures of microtubules and tip-accumulating molecular motors, arXiv:2107.12281.

[10] Xingbo Yang, Matthias Heinemann, Jonathon Howard, Greg Huber, Srividya Iyer-Biswas, Guillaume Le Treut, Michael Lynch, Kristi L. Montooth, Daniel J. Needleman, Simone Pigolotti *et al.*, Physical bioenergetics: Energy fluxes, budgets, and constraints in cells, Proc. Natl. Acad. Sci. U.S.A. **118**, e2026786118 (2021).

[11] Laura Tociu, Étienne Fodor, Takahiro Nemoto, and Suriyanarayanan Vaikuntanathan, How Dissipation Constrains Fluctuations in Nonequilibrium Liquids: Diffusion, Structure, and Biased Interactions, Phys. Rev. X **9**, 041026 (2019).

[12] Viktoria Wollrab, Raghavan Thiagarajan, Anne Wald, Karsten Kruse, and Daniel Riveline, Still and rotating myosin clusters determine cytokinetic ring constriction, Nat. Commun. **7**, 11860 (2016).

[13] Anne-Cécile Reymann, Rajaa Boujemaa-Paterski, Jean-Louis Martiel, Christophe Guérin, Wenxiang Cao, Harvey F. Chin, Enrique M. De La Cruz, Manuel Théry, and Laurent Blanchoin, Actin network architecture can determine myosin motor activity, Science **336**, 1310 (2012).

[14] F. Cagnetta, F. Corberi, G. Gonnella, and A. Suma, Large Fluctuations and Dynamic Phase Transition in a System of Self-Propelled Particles, Phys. Rev. Lett. **119**, 158002 (2017).

[15] Takahiro Nemoto, Étienne Fodor, Michael E. Cates, Robert L. Jack, and Julien Tailleur, Optimizing active work: Dynamical phase transitions, collective motion, and jamming, Phys. Rev. E **99**, 022605 (2019).

[16] Trevor GrandPre, Katherine Klymko, Kranthi K. Mandadapu, and David T. Limmer, Entropy production fluctuations encode collective behavior in active matter, Phys. Rev. E **103**, 012613 (2021).

[17] Avishek Das and David T. Limmer, Variational design principles for nonequilibrium colloidal assembly, J. Chem. Phys. **154**, 014107 (2021).

[18] Hugo Touchette, The large deviation approach to statistical mechanics, Phys. Rep. **478**, 1 (2009).

[19] R. L. Jack, Ergodicity and large deviations in physical systems with stochastic dynamics, Eur. Phys. J. B **93**, 74 (2020).

[20] Udo Seifert, Stochastic thermodynamics, fluctuation theorems and molecular machines, Rep. Prog. Phys. **75**, 126001 (2012).

[21] Étienne Fodor, Robert L. Jack, and Michael E. Cates, Irreversibility and biased ensembles in active matter: Insights from stochastic thermodynamics, Annu. Rev. Condens. Matter Phys. **13**, 215 (2022).

[22] David Wu, Devin L Harrison, Teodora Szasz, Chih-Fan Yeh, Tzu-Pin Shentu, Angelo Meliton, Ru-Ting Huang, Zhengjie Zhou, Gökhan M Mutlu, Jun Huang *et al.*, Single-cell metabolic imaging reveals a SLC2A3-dependent glycolytic burst in motile endothelial cells, Nat. Metab. **3**, 714 (2021).

[23] Thomas Speck, Julian Bialké, Andreas M. Menzel, and Hartmut Löwen, Effective Cahn-Hilliard Equation for the Phase Separation of Active Brownian Particles, Phys. Rev. Lett. **112**, 218304 (2014).

[24] Priti Agarwal and Ronen Zaidel-Bar, Principles of actomyosin regulation *in vivo*, Trends Cell Biol. **29**, 150 (2019).

[25] Florian Huber, Dan Strehle, and Josef Käs, Counterion-induced formation of regular actin bundle networks, Soft Matter **8**, 931 (2012).

[26] Francois Nedelec and Dietrich Foethke, Collective Langevin dynamics of flexible cytoskeletal fibers, New J. Phys. **9**, 427 (2007).

[27] See Supplemental Material http://link.aps.org/supplemental/10.1103/PhysRevLett.129.128002, which includes Refs. [28–30], for details pertaining to numerical simulations, structure characterization, hydrodynamic model and mean-field treatment of dynamical bias, and derivation of the two-state model and prediction of k_{eff}.

[28] Gregory M. Kurtzer, Vanessa Sochat, and Michael W. Bauer, Singularity: Scientific containers for mobility of compute, PLoS One **12**, e0177459 (2017).

[29] Skipper Seabold and Josef Perktold, Statsmodels: Econometric and statistical modeling with python, In *Proceedings of the 9th Python in Science Conference* (2010), Vol. 57, pp. 10–25080.

[30] Joseph L. Doob, *Stochastic Processes*, Wiley classics library edition (Wiley, New York, 1990).

[31] Louise P. Cramer, Margaret Siebert, and Timothy J. Mitchison, Identification of novel graded polarity actin filament bundles in locomoting heart fibroblasts: Implications for the generation of motile force, J. Cell Biol. **136**, 1287 (1997).

[32] Amit Das, Abrar Bhat, Rastko Sknepnek, Darius Koster, Satyajit Mayor, and Madan Rao, Assemblies of F-actin and myosin-II minifilaments: Steric hindrance and stratification at the membrane cortex, bioRxiv, p. 656082 (2019), 10.1101/656082.

[33] Julien Tailleur and Jorge Kurchan, Probing rare physical trajectories with Lyapunov weighted dynamics, Nat. Phys. **3**, 203 (2007).

[34] Takahiro Nemoto, Freddy Bouchet, Robert L. Jack, and Vivien Lecomte, Population-dynamics method with a multicanonical feedback control, Phys. Rev. E **93**, 062123 (2016).

[35] Kripa Gowrishankar and Madan Rao, Nonequilibrium phase transitions, fluctuations and correlations in an active contractile polar fluid, Soft Matter **12**, 2040 (2016).

[36] Nicolás Tizón-Escamilla, Vivien Lecomte, and Eric Bertin, Effective driven dynamics for one-dimensional conditioned Langevin processes in the weak-noise limit, J. Stat. Mech. 01 (2019) 013201.

[37] Hugo Touchette, A basic introduction to large deviations: Theory, applications, simulations, arXiv:1106.4146.

[38] K. Kruse, J. F. Joanny, F. Jülicher, J. Prost, and K. Sekimoto, Generic theory of active polar gels: A paradigm for cytoskeletal dynamics, Eur. Phys. J. E **16**, 5 (2005).

[39] M. C. Marchetti, J. F. Joanny, S. Ramaswamy, T. B. Liverpool, J. Prost, Madan Rao, and R. Aditi Simha, Hydrodynamics of soft active matter, Rev. Mod. Phys. **85**, 1143 (2013).

[40] Thomas Lecuit and Pierre-Francois Lenne, Cell surface mechanics and the control of cell shape, tissue patterns and morphogenesis, Nat. Rev. Mol. Cell Biol. **8**, 633 (2007).